

# CONSISTENCY REGULARISATION FOR UNSUPERVISED DOMAIN ADAPTATION IN MONOCULAR DEPTH ESTIMATION

**Amir El-Ghoussani**

Friedrich-Alexander-Universität Erlangen-Nürnberg  
amir.el-ghoussani@fau.de

**Julia Hornauer**

Ulm University  
julia.hornauer@uni-ulm.de

**Gustavo Carneiro**

University of Surrey  
g.carneiro@surrey.ac.uk

**Vasileios Belagiannis**

Friedrich-Alexander-Universität Erlangen-Nürnberg  
vasileios.belagiannis@fau.de

## ABSTRACT

In monocular depth estimation, unsupervised domain adaptation has recently been explored to relax the dependence on large annotated image-based depth datasets. However, this comes at the cost of training multiple models or requiring complex training protocols. We formulate unsupervised domain adaptation for monocular depth estimation as a consistency-based semi-supervised learning problem by assuming access only to the source domain ground truth labels. To this end, we introduce a pairwise loss function that regularises predictions on the source domain while enforcing perturbation consistency across multiple augmented views of the unlabelled target samples. Importantly, our approach is simple and effective, requiring only training of a single model in contrast to the prior work. In our experiments, we rely on the standard depth estimation benchmarks KITTI and NYUv2 to demonstrate state-of-the-art results compared to related approaches. Furthermore, we analyse the simplicity and effectiveness of our approach in a series of ablation studies. The code is available at <https://github.com/AmirMaEl/SemiSupMDE>.

## 1 INTRODUCTION

Monocular depth estimation plays an active role in computer vision with many applications such as 3D pose estimation, semantic segmentation, and 3D reconstruction. Obtaining accurate depth predictions from a single image, though, is an ill-posed problem, especially in complex indoor and outdoor scenes, due to the ambiguous nature of the inverse depth problem. While the standard supervised learning paradigm, using large annotated depth datasets, have achieved promising performance (Eigen et al., 2014; Laina et al., 2016; Agarwal & Arora, 2023), collecting such data requires extensive resources (Saxena et al., 2009; Gaidon et al., 2016; Handa et al., 2015).

To relax the data annotation requirement, unsupervised learning approaches exploit geometric constraints between multiple views of a scene. For example, stereo-based methods leverage left-right consistency between rectified stereo image pairs to train without explicit depth supervision (Godard et al., 2017; Park & Park, 2022). Such methods require calibrated stereo cameras during both training and inference. Another line of work utilises temporal consistency in video sequences to derive implicit depth cues from camera motion (Zhou et al., 2017; Mahjourian et al., 2018; Zou et al., 2018). While these approaches do not require labelled training data, they are limited to scenarios where stereo imagery or video sequences are available. Furthermore, unsupervised learning methods struggle in situations involving occlusion and object motion (Wang et al., 2018; Sun et al., 2023). In contrast, semi-supervised learning methods utilise a subset of labelled images to directly supervise the model on the depth prediction task (Kuznetsov et al., 2017; Amiri et al., 2019). This guidance is stronger than the indirect cues from multi-view constraints alone in unsupervised learning. More importantly, semi-supervised approaches can leverage unlabelled data along with a limited amount of labelled data, even if stereo or video data is scarce or unavailable in the target domain. However, semi-supervised monocular depth estimation techniques often rely on labelled and unlabelled samples being drawn from the same underlying distribution (Kuznetsov et al., 2017). In practical domain adaptation scenarios, this assumption may not always hold since the labelled source and unlabelled target domains exhibit distribution shifts (Akada et al., 2022; Lopez-Rodriguez & Mikolajczyk, 2020).

To address this issue, recent approaches in monocular depth estimation have explored unsupervised domain adaptation which leverages available labelled source data together with unlabelled target domain images (Yen et al., 2022; Kundu et al., 2018; Zheng et al., 2018; Zhao et al., 2019; Lopez-Rodriguez & Mikolajczyk, 2020).

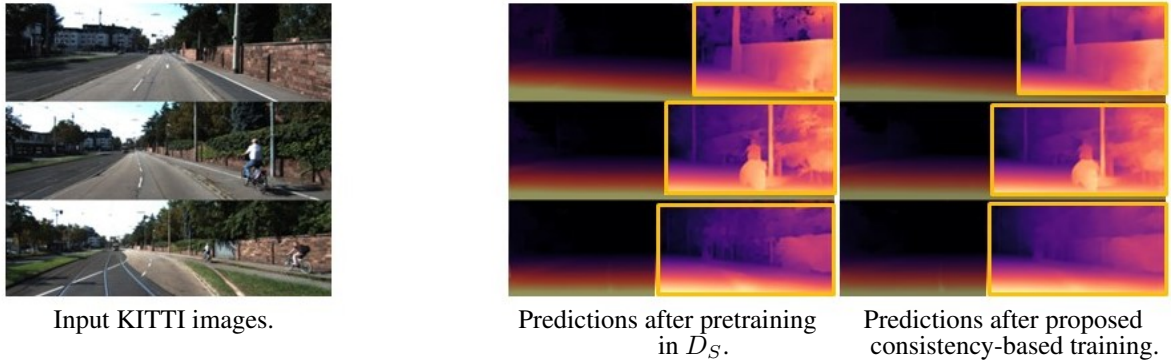


Figure 1: Following pretraining on the source domain using CutMix (Yun et al., 2019) data augmentation, we observe that the resulting depth predictions show some fidelity but could benefit from further refinement in certain areas. Specifically, they appear overly fragmented or “edgy” in localised regions (highlighted in the figure). Based on this observation we carefully design our consistency-based approach for domain adaptation in monocular depth estimation, to particularly smooth localised and fragmented regions.

In particular, unsupervised domain adaptation techniques leverage labelled source data to guide prediction in unlabelled target domains by aligning representations across domains (Qiu & Yuille, 2016; Shrivastava et al., 2017). These are the key capabilities that we also aim to explore in this work. Existing domain adaptation approaches for monocular depth estimation mainly rely on self-supervised or unsupervised techniques using consistency-based (Zheng et al., 2018; Xie et al., 2016; Zhou et al., 2017) or geometry-based (Yen et al., 2022; Yin et al., 2018) losses. While consistency methods provide a general constraint using simple transformations, geometry models require additional meta-data, e.g., camera intrinsics, that may be unavailable for new unlabelled target domains. Similarly, our approach also falls into the first category of consistency-based approaches. In contrast to prior consistency-based works that focused only on target-domain consistency regularisation, we incorporate supervised information by matching predictions on the target and source images simultaneously. Additionally, we employ consistency regularisation for the purpose of unsupervised domain adaptation by requiring target predictions to remain coherent when propagated through multiple augmentation streams. To our knowledge this represents the first application of a technique using both multi-stream target consistency and source-based regularisation for domain adaptive monocular depth estimation.

Furthermore, the existing domain adaptation approaches often involve complex multi-stage optimising various geometric and photometric losses modelling camera motion or stereo correspondences (Zou et al., 2018; Mahjourian et al., 2018), leading to optimisation challenges. For example, external models such as semantic segmentation models are used to enforce semantic consistency (Lopez-Rodriguez & Mikolajczyk, 2020) or 3D point cloud models (Yen et al., 2022) are employed for pseudo label generation, ultimately increasing dependencies. In contrast, we present an approach to train only the depth estimation model and require no additional trainable models, keeping the training procedure simple. Additionally, target and source data are typically optimised separately for the above methods without an explicit linking of predictions across domains. In comparison, we propose to simultaneously optimise the supervised source objective and the unsupervised target objective in a single training stage.

In this work, we formulate the problem of unsupervised domain adaptation for monocular depth estimation as a consistency-based semi-supervised learning problem. We present a semi-supervised approach for training a single model by assuming access only to the labels of the source domain data. Initially, we conduct supervised pre-training using heavily augmented labelled source data to obtain preliminary depth predictions. Afterwards, depth maps predicted on unlabelled target domain data are used as pseudo-labels. Our approach is motivated by the fact that after the initial pre-training in the source domain, the depth predictions appear somewhat faithful but are still edgy and fragmented in certain areas (see Fig. 1). This suggests that additional refinement of object boundaries and detection of previously missing objects could improve the overall depth map quality. To that end, we introduce a pairwise loss term that regularises the predictions on the source domain to be consistent with the ground truth depth distribution in the source domain, while simultaneously enforcing multiple perturbation consistency during pseudo-labelling on the target domain. We assess the performance of our method in two standard domain adaptation benchmarks with indoor and outdoor datasets, where Virtual KITTI (Gaidon et al., 2016) / SceneNet (Handa et al., 2015) are the source domains and KITTI (Geiger et al., 2013) / NYU (Nathan Silberman & Fergus, 2012) are the corresponding target domains.

Our main contributions can be summarised as follows:

- We present a semi-supervised approach for unsupervised domain adaptation by introducing a pairwise loss that regularises the predictions on the source domain, while simultaneously enforcing perturbation consistency across multiple augmented views of unlabelled target data.
- Importantly, we do not require any additional trainable models, making the proposed method simple and effective. To the best of our knowledge, we are the first to develop domain adaptation by simultaneous optimisation using source and target data in one training stage.
- In the extensive evaluation based on the standard depth estimation benchmarks KITTI (Geiger et al., 2013) and NYU (Nathan Silberman & Fergus, 2012), our proposed method demonstrates state-of-the-art performance in the domain adaptation task.

## 2 RELATED WORK

### 2.1 MONOCULAR DEPTH ESTIMATION

Monocular depth estimation consists of predicting the depth information of a scene from a single image. With the rapid development of deep neural networks, monocular depth estimation with the help of deep learning has been widely studied. Various supervised learning approaches have been proposed in recent years for monocular depth estimation. Eigen et al. (Eigen et al., 2014) propose a CNN-based approach to directly regress the depth. Liu et al. (Liu et al., 2016) propose utilising a fully-connected CRF as a post-processing step to refine monocular depth predictions. Other methods have extended the CNN-based network by changing the regression loss to a classification loss (Cao et al., 2016; Fu et al., 2018; Peng Wang et al., 2015; Yin et al., 2019; Bhat et al., 2021) or change the architecture of the depth estimation network entirely (Liu et al., 2023; Rudolph et al., 2022). In addition, a number of self-supervised techniques have been proposed to train monocular depth estimation models without relying on ground truth labels. GeoNet (Yin et al., 2018) enforces epipolar geometry consistency, and DF-Net (Zou et al., 2018) models rigid scene flow. SfMLearner (Zhou et al., 2017) explores photometric alignment. Godard et al. (2017) use stereo consistency between synchronised camera views for unsupervised monocular depth estimation. More recently, attention-based architectures have achieved new performance milestones in monocular depth estimation. DepthFormer adopted Vision Transformers for strong multi-scale representations (Lin et al., 2020). Similarly, DPT fused CNNs and self-attention in a hybrid network (Ranftl et al., 2021). Neural Window Fully Connected CRFs (Yuan et al., 2022) introduced CRF modelling in a neural window, leveraging pixel-level affinity and semantic connections to refine initial depth maps. Agarwal & Arora (2023) propose a novel architecture that utilises skip attention to refine pixel-level queries and improve depth predictions. While supervised learning approaches have achieved considerable success in monocular depth estimation tasks, acquiring large annotated depth datasets at scale remains challenging. Self-supervised methods provide an alternative, but traditional techniques depend on camera parameters and frame geometries, which often do not hold strictly in real-world settings. Furthermore, the lack of direct supervision signals hinders the ability of self-supervised models to fully leverage available visual cues.

### 2.2 DOMAIN ADAPTATION FOR DEPTH ESTIMATION

Domain adaptation techniques leverage synthetic data as a labelled source domain and unlabelled real data as the target domain for monocular depth estimation (Chen et al., 2019; Kundu et al., 2018; Lopez-Rodriguez & Mikolajczyk, 2020; PNVR et al., 2020; Zhao et al., 2019; Zheng et al., 2018; Yen et al., 2022). Most prior approaches treat depth estimation as a regression task while relying on style- or image translation for pixel-level adaptation (Atapour Abarghouei & Breckon, 2018), adversarial learning for feature-level adaptation (Kundu et al., 2018; Hornauer et al., 2021), or a combination of both (Zheng et al., 2018; Zhao et al., 2019). For instance, AdaDepth (Kundu et al., 2018) aligns source and target distributions in features and predictions.  $T^2Net$  (Zheng et al., 2018) extends this idea by adopting both synthetic-to-real translation network and feature alignment in the task network. However, aligning features were found to be ineffective in outdoor datasets despite promising improvements observed when training on real stylised images (Zheng et al., 2018). 3D-PL (Yen et al., 2022) combines domain adaptation, pseudo-labelling and 3D-awareness to improve the depth estimation performance in a target domain. These methods leverage the geometric information present in depth maps to generate more accurate pseudo-labels. Other follow-up methods have explored bidirectional translation (real-to-synthetic and synthetic-to-real) and utilise depth consistency loss on the predictions between real and real-to-synthetic images (Zhao et al., 2019; Chen et al., 2021). GASDA (Zhao et al., 2019) incorporates additional information: it utilises stereo pairs to encourage geometry consistency and align stereo images for depth estimation. Similarly, SharinGAN (PNVR et al., 2020) maps domains to a shared space with geometry constraints. Moreover, DESC (Lopez-Rodriguez & Mikolajczyk, 2020) adopts segmentation for pseudo-labeling based on instance properties. Our approach to domain adaptation for depth estimation offers several advantages compared to

existing methods. Specifically, our method provides direct pseudo-labels on real data in a simple and straightforward manner, without the need for any external information, such as semantic information (Lopez-Rodriguez & Mikolajczyk, 2020). Additionally we leverage labeled source data by simultaneously optimizing on target and source domain images.

### 2.3 SEMI-SUPERVISED LEARNING

There are two main methodologies used in semi-supervised learning, namely entropy minimisation and consistency regularisation. Entropy minimisation involves self-training on pseudo labels for unlabelled data. Conversely, consistency regularisation assumes predictions should remain stable under perturbations. Among the consistency regularisation methods, FixMatch (Sohn et al., 2020) proposes using strong perturbations for unlabelled images and supervising the training process with predictions from weakly perturbed images, combining the benefits of both approaches. Recent advancements like FlexMatch (Zhang et al., 2021) and FreeMatch (Wang et al., 2022) consider class-wise confidence thresholds. In Yang et al. (2023), UniMatch is proposed, which aims to improve the performance of semi-supervised semantic segmentation by incorporating extra information and imposing constraints on real images. Our work takes inspiration from these semi-supervised learning techniques that leverage consistency regularisation principles. However, these approaches have primarily focused on classification and segmentation tasks with discrete label spaces. As monocular depth estimation produces continuous-valued depth maps, it poses a regression problem rather than classification or segmentation. Inspired by FixMatch (Sohn et al., 2020), we propose a framework for semi-supervised monocular depth estimation. Specifically, we formulate depth prediction as regression and design augmentations and consistency losses suitable for continuous outputs.

## 3 METHOD

Let  $f(\mathbf{x}; \theta)$  denote a neural network parameterised by  $\theta$  that maps the input image  $\mathbf{x} \in \mathbb{R}^{h \times w \times 3}$  to the depth prediction  $\hat{y} \in \mathbb{R}^{h \times w \times 1}$ . The depth estimation model  $f(\cdot)$  is trained on the source domain  $D_S$  containing images  $\mathbf{x}_s$  with corresponding ground truth depth maps  $\mathbf{y}_s$ , and the target domain  $D_T$  of images  $\mathbf{x}_u$  without accompanying depth labels. Directly optimising  $f(\cdot)$  based solely on supervised losses in the source domain  $D_S$  would lead to degraded performance when applied to the unlabelled target domain  $D_T$ , owing to the domain gap between the source and the target data distributions.

To address this issue, we propose a semi-supervised learning approach that facilitates direct supervision on the target image  $\mathbf{x}_u$ , thereby effectively reducing the domain gap. Initially, we train the depth prediction model  $f(\cdot)$  using source domain data. After this pre-training, we train our model by enforcing perturbation consistency across augmented views in  $D_T$  while also optimising on supervised source data using a new pairwise loss. Critically, we simultaneously apply both loss terms during training, allowing source supervision to guide pseudo-label refinement while the proposed consistency across target perturbations induces adaptation.

**Preliminaries** We derive inspiration by FixMatch (Sohn et al., 2020) in which each unlabelled sample undergoes simultaneous perturbations by two operators: a weak perturbation such as cropping and a strong perturbation like colour jittering. Weak perturbations are generally augmentations, that minimally alter the scene content, while strong perturbations introduce more distortion and artefacts. The overall objective function is a combination of supervised loss  $\mathcal{L}^s$  and unsupervised loss  $\mathcal{L}^u$ , given by:

$$\mathcal{L} = \frac{1}{2}(\mathcal{L}^s + \mathcal{L}^u) \quad (1)$$

Typically the supervised term  $\mathcal{L}_s$  is a cross-entropy loss between the model predictions and the labels. The unsupervised loss  $\mathcal{L}_u$  serves to regularise the prediction of the sample under strong perturbations to be the same as that under weak perturbations.

Based on Eq. 1, we present a formulation for the monocular depth estimation setting.

We propose to replace the supervised loss  $\mathcal{L}^s$  with a pairwise loss  $\mathcal{L}_\Sigma^s$ , applied to source domain samples in  $D_S$ , while also extending  $\mathcal{L}^u$  with perturbation consistency across three augmented views in the target domain  $D_T$ .

### 3.1 PERTURBATION CONSISTENCY

We seek to minimise the differences between predictions on augmented versions of the same input image. Due to the unsupervised domain adaptation setting where no depth annotation for the target domain is available, we rely on enforcing consistency between multi-stream perturbed image predictions in the target domain. For each input sample,



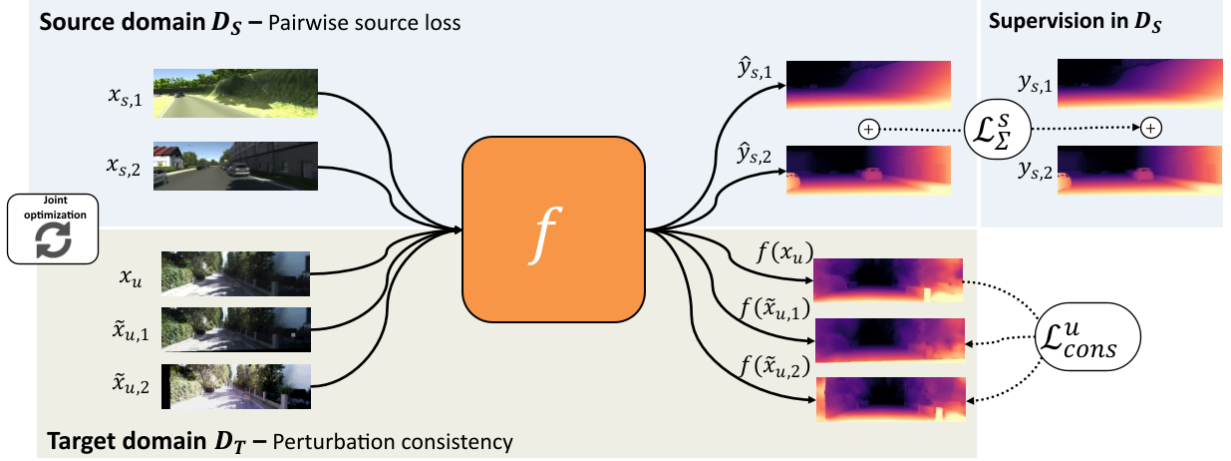


Figure 2: Overview of the approach. Initially, we sample two independent source domain images  $\mathbf{x}_{s,1}$  and  $\mathbf{x}_{s,2}$  along with one target domain image  $\mathbf{x}_u$ . This target domain image is then fed into two perturbation streams, in which independent augmentations are applied to the target image, denoted as  $\tilde{\mathbf{x}}_{u,1}$  and  $\tilde{\mathbf{x}}_{u,2}$ . In total five samples are concatenated and fed into the depth estimation model  $f(\cdot)$ . Afterwards, the predictions are chunked back into their initial shapes. The loss on the supervised domain is computed by enforcing consistency between the sum of predictions and the sum of the two ground truth samples. Finally, the unsupervised loss is calculated by enforcing consistency between generated perturbations. Yellow and blue colors correspond to the supervised source and the unsupervised target domain, respectively.

we apply the RandAugment (Cubuk et al., 2019) algorithm to generate multiple perturbed views, or ”streams”, of the data. Each augmentation chain is applied independently to a target sample  $\mathbf{x}_u$  to produce uniquely transformed versions of the input. In total, we generate two augmented versions of the image, in addition to the initial unlabelled target domain image  $\mathbf{x}_u$ :

$$\tilde{\mathbf{x}}_{u,1} = RA_{Depth,1}(\mathbf{x}_u), \quad (2)$$

$$\tilde{\mathbf{x}}_{u,2} = RA_{Depth,2}(\mathbf{x}_u), \quad (3)$$

where  $RA_{Depth,1}$  and  $RA_{Depth,2}$  represent independent RandAugment operations. The multi-stream perturbed images  $\tilde{\mathbf{x}}_{u,1}$  and  $\tilde{\mathbf{x}}_{u,2}$  along with an initial sample  $\mathbf{x}_u$  are then fed through the depth estimation model  $f(\cdot)$  to obtain three predicted depth maps. All three depth predictions should be consistent; therefore, we compute the  $\mathcal{L}_1$  loss between the predicted depth maps to enforce consistency:

$$\mathcal{L}_{cons}^u = \sum_{i=1}^N \|f(\mathbf{x}_{u,i}) - f(\tilde{\mathbf{x}}_{u,1,i})\|_1 + \|f(\mathbf{x}_{u,i}) - f(\tilde{\mathbf{x}}_{u,2,i})\|_1,$$

where  $N$  is the batch size. We empirically observed that two augmented versions of each unlabelled sample provided the best trade-off between boosting performance via view redundancy and managing memory costs. Moreover, prior work on semi-supervised learning has shown that generating multiple perturbed views of unlabelled data strengthens consistency regularisation (Berthelot et al., 2019; Caron et al., 2020).

### 3.2 PAIRWISE LOSS

While the unsupervised perturbation consistency adapts the model to the target domain without source supervision, there is no way to directly assess the quality and accuracy of pseudo-labels  $f(\mathbf{x}_u)$ ,  $f(\tilde{\mathbf{x}}_{u,1})$  and  $f(\tilde{\mathbf{x}}_{u,2})$ . Errors can accumulate during training as the network learns potentially incorrect target predictions. For that reason, we regularise the training process, leveraging a pairwise loss  $\mathcal{L}_{\Sigma}^s$  in the source domain  $D_S$ . Specifically, for each source domain batch we sample image pairs  $(\mathbf{x}_{s,1}, \mathbf{x}_{s,2})$  along with their corresponding depth annotations  $(\mathbf{y}_{s,1}, \mathbf{y}_{s,2})$ , and then compute the  $\mathcal{L}_1$  distance between the sum of predictions and labels over a batch of size  $N$ :

$$\hat{\mathbf{y}}_{s,1} = f(\mathbf{x}_{s,1}), \quad \hat{\mathbf{y}}_{s,2} = f(\mathbf{x}_{s,2}) \quad (4)$$

$$\hat{\mathbf{y}}_{\Sigma,s} = \hat{\mathbf{y}}_{s,1} + \hat{\mathbf{y}}_{s,2} \quad (5)$$

$$\mathbf{y}_{\Sigma,s} = \mathbf{y}_{s,1} + \mathbf{y}_{s,2} \quad (6)$$

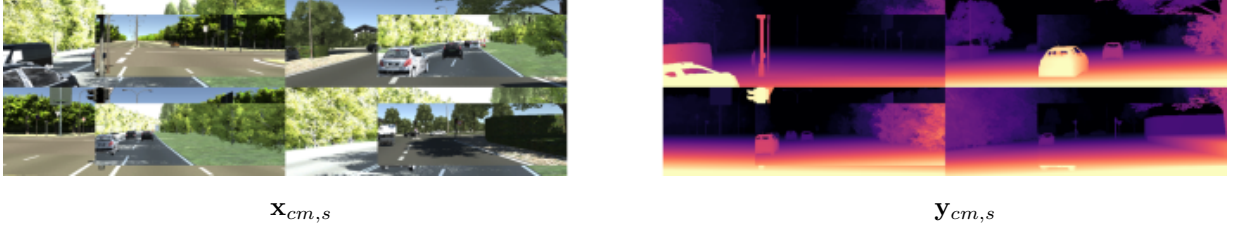


Figure 3: CutMix augmented input images  $\mathbf{x}_{cm,s}$  in the source domain along with their corresponding augmented ground truth depth annotation  $\mathbf{y}_{cm,s}$ . We choose  $\alpha = 0.5$ , controlling the patch size of the CutMix augmentation.

$$\mathcal{L}_{\Sigma}^s = \sum_{i=1}^N \|\mathbf{y}_{\Sigma,s,i} - \hat{\mathbf{y}}_{\Sigma,s,i}\|_1. \quad (7)$$

A key observation from our experiments is that the proposed pairwise source regularisation approach from the source domain labels requires using an extremely low learning rate for stable optimisation. Since already seen images are combined in new configurations during each summation, essentially, this approach ends up augmenting the training data online.

### 3.3 COMPLETE LOSS FUNCTION

In total, we propose a loss formulation that combines the multiple perturbation consistency constraints imposed on unlabelled target samples with the proposed summation-based pairwise loss computed on the labelled source samples. It is given by:

$$\mathcal{L}_{total} = \frac{1}{2} \sum_i^N (\mathcal{L}_{\Sigma,i}^s + \mathcal{L}_{cons,i}^u) \Big|_{r=2}. \quad (8)$$

where  $N$  denotes the batch size. Additionally, we introduce the batch ratio hyperparameter  $r = \frac{n_{supervised}}{n_{unsupervised}}$  to balance the amount of supervised vs. unsupervised training data. A ratio parameter 2 indicates that twice as many supervised as unsupervised samples were used during one forward pass (an exact calculation of the total amount of samples in one forward pass with  $N = 12$  and  $r = 2$  is shown in the appendix, in Eq. 15). An ablation (see Table 4, in Sec. 4.3) examines various  $r$  values, revealing a static value of 2 outperforms other schemes.

### 3.4 MODEL PRETRAINING

During model pre-training, images from one single batch are mixed with one another using CutMix (Yun et al., 2019) augmentations. This prevents the depth estimation model from relying too heavily on local image details, as it forces the model to consider information from different regions. We apply CutMix to all source samples  $\mathbf{x}_s$  and their corresponding annotations  $\mathbf{y}_s$  during pretraining. CutMix randomly combines two different images by cutting out a random patch from one image and replacing it with the same-sized patch from another image. The corresponding ground truth labels are also mixed in proportion to the area of the patches, defined by a hyperparameter  $\alpha$ . Fig. 3 illustrates this procedure for the virtual KITTI source dataset (Gaidon et al., 2016). We then compute the  $\mathcal{L}_1$ -distance between depth predictions of these augmented samples  $\tilde{\mathbf{x}}_{cm,s}$  and their corresponding ground truth depth annotation  $\tilde{\mathbf{y}}_{cm,s}$  over the batch of size  $N$ :

$$\mathcal{L}^s = \sum_{i=1}^N \|f(\tilde{\mathbf{x}}_{cm,s,i}) - \tilde{\mathbf{y}}_{cm,s,i}\|_1. \quad (9)$$

## 4 EXPERIMENTS

We assess our method on two challenging benchmarks, one indoors and one outdoors. Afterwards, we conduct detailed ablation studies on each benchmark to analyse the importance of the different components in our approach.

#### 4.1 DATASETS

**Outdoor** We utilise the virtual KITTI (vKITTI) (Gaidon et al., 2016) dataset, with 21,260 synthetic image-depth pairs as our labeled source domain, and the real KITTI dataset (Geiger et al., 2013), containing 22,600 images as the unlabeled target domain. As vKITTI and KITTI contain outdoor street scenes, we preprocessed both and clip maximum depth values to 80 m to ensure consistency when applying our approach during training, similar to (Zheng et al., 2018). Following prior works (Zheng et al., 2018; Yen et al., 2022; Zhao et al., 2019), we evaluate the performance on the Eigen test split (Eigen et al., 2014). For the final test evaluation, we use the Garg crop (Garg et al., 2016) and clamp the ground truth depth to 50 m and 80 m following prior work (Yen et al., 2022).

**Indoor** For our second experiment, we employ the large-scale SceneNet synthetic dataset (Handa et al., 2015) as the source and evaluated the real-world NYUv2 (Nathan Silberman & Fergus, 2012) indoor dataset as the target domain. Additionally, we apply a filtering procedure to the SceneNet dataset to better match the characteristics of NYUv2. Specifically, we aim to resemble the depth distribution of NYUv2, as SceneNet is considerably larger. After filtering, our source SceneNet set contains 4,737 samples. We combine this filtered SceneNet set with a randomly selected subset of 5,000 samples from the raw NYUv2 data as our target domain samples. By selecting a target domain subset of similar size to our source domain set, we aim to keep the ratio of unsupervised to supervised samples close to 1 : 1 during training.

Given these datasets capture indoor room layouts and objects, significantly shorter maximum depths are present. Therefore, we clip the maximum depth to 8 m for this indoor adaptation problem, following prior work (Zheng et al., 2018). Our final evaluation is then performed on the Eigen split (Eigen et al., 2014) of the NYU depth data, clipped to 8 m.

**Implementation details** We adopt a U-Net like (Ronneberger et al., 2015) architecture similar to Zheng et al. (2018) as our depth prediction model  $f(\cdot)$ . The model is trained on an NVIDIA GTX 6000 GPU using the Adam optimizer (Kingma & Ba, 2014), pretraining is done with a learning rate of  $4 * 10^{-3}$  for 250 epochs while our domain adaptation is applied at learning rate of  $4 * 10^{-8}$  for 10 epoch with a linear decay after 4 epochs. In total pretraining takes about six hours for the outdoor benchmarks and about one hour for the indoor benchmarks.

**Evaluation metrics** Consistent with previous research (Yen et al., 2022; Zheng et al., 2018; Kundu et al., 2018; Zhao et al., 2019), we assess unsupervised domain adaptation for monocular depth prediction. To evaluate the adapted depth estimation model, we utilize common metrics, including absolute relative error (AbsRel), root mean squared error (RMSE), squared relative error (SqRel), logarithm of root mean squared error (RMSE Log), and accuracy under different threshold values ( $A1$  at threshold  $\delta < 1.25$ ,  $A2$  at  $\delta < 1.25^2$  and  $A3$  at  $\delta < 1.25^3$ ).

**Comparison to Related Work** For a fair evaluation, we compare to prior work using analogous experimental protocols. Specifically, we benchmark against fully-supervised methods training on single domains (Eigen et al., 2014; Liu et al., 2016). We also compare to baselines trained on separate source/target distributions without adaptation. Critically, we evaluate against prominent unsupervised domain adaptation methods (Kundu et al., 2018; Zheng et al., 2018; Yen et al., 2022) which similarly utilise unlabelled target data through depth completion or translation. These prior works employ architectures and datasets matching our setup, allowing an effective and fair assessment of our approach. The works of SharingGAN (PNVR et al., 2020) and GASDA (Zhao et al., 2019) report results when leveraging stereo imagery under the assumption that epipolar geometry constraints can be imposed. Consequently we do not compare our approaches to theirs.

#### 4.2 RESULTS

**Outdoor experiments** Table 1 shows quantitative results where we compare our approach to various baselines and state-of-the-art approaches with ground truth depth labels clipped to 80 m. In addition, we compare to 'all-synthetic' and 'all-real' baselines, referring to the approaches where the model is trained on synthetic or real data only. These can be seen as the upper and lower bound, respectively. We also provide quantitative results capped to 50 m in Table 2. In this setup, we compare to the supervised approach proposed by Garg et al. (Garg et al., 2016). In comparison to the standard supervised training baseline 'all-synthetic', our method outperforms this baseline by a significant margin. We further compare to three previous state-of-the-art semi-supervised depth estimation techniques. Notably, our approach achieves a significant improvement in  $A1$ -accuracy compared to prior work and outperforms 3D-PL (Yen et al., 2022) in all metrics.

Table 1: Results on the KITTI Eigen split (80m cap) for single image depth estimation methods. The column ‘supervised’ determines whether an approach has been trained with target image ground truth samples. ‘K’ refers to KITTI, ‘S’ to the vKITTI and ‘CS’ to Cityscapes data. ‘DA’ refers to domain adaptation approaches.

Method	Supervised	Dataset	AbsRel↓	SqRel↓	RMSE↓	RMSE log↓	A1↑	A2↑	A3↑
Eigen et al. (2014)	Yes	K	0.203	1.548	6.307	0.282	0.702	0.890	0.958
Liu et al. (2016)	Yes	K	0.202	1.614	6.523	0.275	0.678	0.895	0.965
Zhou et al. (2017)	No	K	0.208	1.768	6.856	0.283	0.678	0.885	0.957
Zhou et al. (2017)	No	K+CS	0.198	1.836	6.565	0.275	0.718	0.901	0.960
All synthetic	No	S	0.253	2.303	6.953	0.328	0.635	0.856	0.937
All real	No	K	0.158	1.151	5.285	0.238	0.811	0.934	0.970
Kundu et al. (2018)	No	K+S(DA)	0.214	1.932	7.157	0.295	0.665	0.882	0.950
Zheng et al. (2018)	No	K+S(DA)	0.182	1.611	6.216	0.265	0.749	0.898	0.959
Yen et al. (2022)	No	K+S(DA)	0.169	1.371	6.037	0.256	0.759	0.904	<b>0.961</b>
Ours	No	K+S(DA)	<b>0.168</b>	<b>1.347</b>	<b>6.002</b>	<b>0.254</b>	<b>0.769</b>	<b>0.907</b>	<b>0.961</b>

Table 2: Results on the KITTI Eigen split capped to 50m. ‘K’ refers to KITTI, ‘S’ to the vKITTI and ‘CS’ to Cityscapes data. ‘DA’ refers to domain adaptation approaches.

Method	Dataset	AbsRel↓	SqRel↓	RMSE↓	RMSE log ↓	A1↑	A2↑	A3↑
Garg et al. (2016)	K	0.169	1.080	5.104	0.273	0.740	0.904	0.962
All synthetic	S	0.244	1.771	5.354	0.313	0.647	0.866	0.943
All real	K	0.151	0.856	4.043	0.227	0.824	0.940	0.973
Kundu et al. (2018)	K+S(DA)	0.203	1.734	6.251	0.284	0.687	0.899	0.958
Zheng et al. (2018)	K+S(DA)	0.168	1.199	4.674	0.243	0.772	0.912	0.966
Yen et al. (2022)	K+S(DA)	0.162	1.049	4.463	0.239	0.776	0.916	<b>0.968</b>
Ours	K+S(DA)	<b>0.161</b>	<b>1.028</b>	<b>4.449</b>	<b>0.237</b>	<b>0.785</b>	<b>0.918</b>	<b>0.968</b>

**Indoor experiments** To further assess model generalisation, we conduct additional experiments in an indoor domain transfer setting. Specifically, we benchmark our approach against a baseline experiment ‘all-synthetic’, trained only on supervised source data, and T2Net (Zheng et al., 2018). However, as our experimental protocol evaluates a novel SceneNet-to-NYUv2 domain shift scenario not explored in the original work, it was necessary to retrain T2Net’s framework for direct comparison. As shown in Table 3, our approach significantly outperforms training the ‘all-synthetic’ baseline, trained without leveraging unlabelled NYUv2 data. Remarkably, we achieve gains over the prior work (Zheng et al., 2018) across most metrics. We outperform Zheng et al. (2018)’s approach in every metric except the Absolute Relative Error.

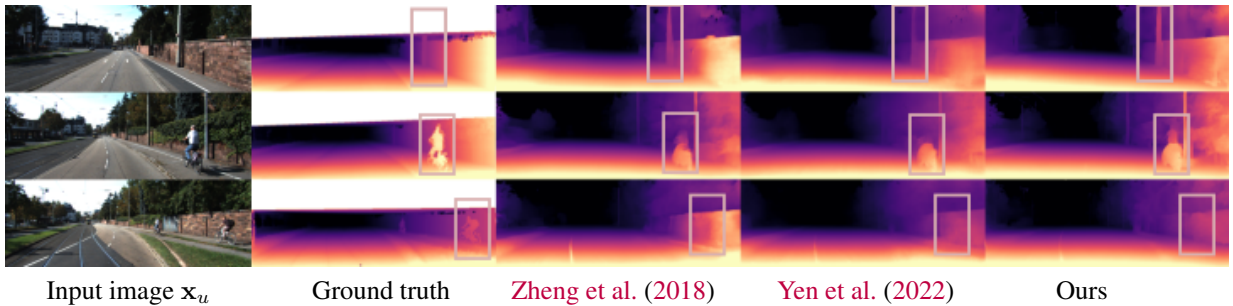


Figure 4: Qualitative results on KITTI (Geiger et al., 2013) with models trained on vKITTI-KITTI. Ground truth depth is linearly interpolated for visualization.

**Qualitative results** In this setting, we compare our approach trained on the vKITTI-KITTI domain adaptation task and test it on the KITTI Eigen split (Eigen et al., 2014) with previous state-of-the-art methods (Yen et al., 2022; Zheng et al., 2018). Fig. 4 shows that our approach better recovers fine-grained depth details in several examples. In particular, in the upper row our approach produces more accurate results for the lamp post. Similarly, in the second row our approach is capable of detecting the cyclist entirely, compared to 3D-PL.

**Limitations** A key limitation of our approach is its reliance on synthetic depth maps possessing well-defined edges in the source domain. Due to the discontinuities at object boundaries present in these rendered depth maps, they differ



Table 3: Results of our approach on the NYU Eigen split capped at 8m. 'N' refers to NYU data, 'S' refers to SceneNet data and 'DA' corresponds to domain adaptation.

Method	Dataset	AbsRel↓	SqRel↓	RMSE↓	RMSE log ↓	A1↑	A2↑	A3↑
all-real	N	0.201	0.252	0.789	0.288	0.609	0.862	0.956
all-synthetic	S	0.432	0.720	1.183	0.439	0.395	0.686	0.859
Zheng et al. (2018)	N+S(DA)	<b>0.394</b>	0.613	1.156	0.417	0.407	0.707	0.878
Ours	N+S	0.417	<b>0.601</b>	<b>1.055</b>	<b>0.385</b>	<b>0.426</b>	<b>0.725</b>	<b>0.890</b>

from real-world captured depth maps which typically exhibit smoother transitions at edges. The edge characteristics between our synthetic source depth maps and target domain data, which lacks such discontinuities, introduces a domain shift that our method seeks to overcome via target-domain consistency regularisation and source-based regularisation. A key assumption of our approach is therefore that the edge characteristics of depth maps in the target and source domains differ sufficiently.

Another key limitation of the proposed approach stems from its computational demands (see also Tab. 9). The framework enforces consistency across multiple augmented views of target images as well as a supervised pairwise loss in the source domain. This joint optimisation comes at the cost of increased computational complexity. Scaling the framework to high-resolution imagery or large datasets would require more expensive GPU hardware.

#### 4.3 ABLATION STUDIES

Next, we analyse several key hyper-parameters involved in our proposed methodology. First, we explore the effect of varying the ratio parameter  $r$ .

Next, we evaluate different data augmentation techniques to understand their impact on our model's ability when no source domain samples are provided.

**Importance of the ratio  $r$**  The balance between unlabelled target consistency training samples and labelled source supervision samples is determined by the ratio  $r$ . To evaluate the importance of this hyperparameter, we conduct an ablation study examining different constant sampling ratios. The quantitative results presented in Table 4 indicate the sensitivity of our approach to the ratio hyperparameter  $r$ . Peak performance was observed for a ratio of  $r = 2/1$ , where twice as many supervised source images as unsupervised target images were sampled within each batch. Hyperparameters were chosen based on the obtained uncertainty  $u$  (For a more detailed explanation please refer to 4.3). Additionally, the effect of the ratio  $r$  on the level of regularisation can be observed. A ratio  $r \approx 1$  leads to weaker regularisation, as evidenced by the higher absolute and squared relative errors achieved with lower  $r$  values. This is understandable, as a lower  $r$  places less importance on the paired source loss term during training, therefore providing less regularisation pressure.

Table 4: Ablation study of our approach with ratio hyperparameter  $r$ . All approaches are capped to 50m.

ratio $r$	AbsRel↓	SqRel↓	RMSE↓	RMSE log ↓	A1↑	A2↑	A3↑	Uncertainty $u$
7/4	0.170	1.092	<b>4.406</b>	0.241	0.783	0.918	0.967	216.83
9/2	0.169	1.115	4.437	0.240	0.783	0.918	0.967	198.83
6/5	0.183	1.441	4.635	0.252	0.775	0.912	0.963	219.29
8/15	0.176	1.153	4.414	0.243	0.779	0.915	0.966	210.15
2/1	<b>0.161</b>	<b>1.028</b>	4.449	<b>0.237</b>	<b>0.785</b>	<b>0.918</b>	<b>0.968</b>	<b>170.73</b>

**Comparison with different loss functions** Next, we conducted an additional experimental comparison using the virtual KITTI (vKITTI) (Gaidon et al., 2016) and real KITTI (Geiger et al., 2013) datasets (see Tab. 5). We compare our method to a standard baseline inspired by FixMatch (Sohn et al., 2020) that only leverages data augmentations within the target KITTI domain, i.e., without considering our multi-stream perturbation consistency losses. Note: all experiments in Tab. 5 are conducted without using the pairwise source loss  $\mathcal{L}_{\Sigma}^s$  except from the experiment 'Ours' in the last row. In particular, we evaluate a setup using strong color-space augmentations only, and compare to RandAugment's geometric transformations. No weak augmentations were applied in all these setups.

The ablation study allowed us to assess the benefits of including geometric augmentations into our approach. Our experimental findings indicate that semi-supervised techniques for depth estimation consistently outperform direct

pretraining (see the "all synthetic" experiment in Tab. 2) without additional adaptation or regularisation. However, incorporating geometric data augmentations into the consistency regulariser provides a substantial boost in performance. Overall, our complete approach shows considerable improvements on the absolute relative error and squared relative error - two key metrics for assessing depth estimation accuracy.

Table 5: Ablation study: comparison with FixMatch (Sohn et al., 2020) baselines. All approaches are capped to 50m and all experiments are subjected to pre-training.

Method	AbsRel↓	SqRel↓	RMSE↓	RMSE log ↓	A1↑	A2↑	A3↑
Colorspace perturbations in $D_T$	0.183	1.393	4.697	0.250	0.775	0.912	0.964
RandAugment perturbations in $D_T$	0.172	1.159	4.475	0.239	0.781	0.916	0.965
Ours with $\mathcal{L}_{\Sigma}^s$	<b>0.161</b>	<b>1.028</b>	<b>4.449</b>	<b>0.237</b>	<b>0.785</b>	<b>0.918</b>	<b>0.968</b>

**Significance of combining  $\mathcal{L}_{\Sigma}^s$  and  $\mathcal{L}_{cons}^t$**  To determine the effectiveness of our proposed approach combining source loss  $\mathcal{L}_{\Sigma}^s$  and target loss  $\mathcal{L}_{cons}^t$  we conduct an ablation study using the losses separately (see Tab. 6).

Table 6: Comparison of our approach when combining and separating both the source loss  $\mathcal{L}_{\Sigma}^s$  and the target loss  $\mathcal{L}_{cons}^t$ .

Losses	AbsRel↓	SqRel↓	RMSE↓	RMSE log↓	A1↑	A2↑	A3↑
with $\mathcal{L}_{\Sigma}^s, \mathcal{L}_{cons}^t$	<b>0.161</b>	<b>1.028</b>	<b>4.449</b>	<b>0.237</b>	<b>0.785</b>	<b>0.918</b>	<b>0.968</b>
with $\mathcal{L}_{cons}^t$	0.171	1.178	4.544	0.248	0.781	0.912	0.965
with $\mathcal{L}_{\Sigma}^s$	0.178	1.356	5.040	0.258	0.779	0.912	0.961
Only pretraining	0.173	1.413	5.062	0.264	0.767	0.906	0.957

These results reveal that the primary driver of the model’s enhanced performance is the unsupervised consistency loss enforced on target perturbations (i.e.  $\mathcal{L}_{cons}^t$ ). Specifically, the pairwise loss on the source domain (i.e.  $\mathcal{L}_{\Sigma}^s$ ) alone provides only minimal regularisation benefits compared to the baseline. However, when combining both proposed objectives, we observe more noticeable gains according to certain error metrics such as absolute relative error (Abs Rel) and root mean squared error of the logarithm (RMSE log). This suggests that jointly leveraging source supervision together with unsupervised consistency across target transformations produces a regularisation effect superior to utilising either loss separately.

## 5 CONCLUSION

We formalised the problem of unsupervised domain adaptation for monocular depth estimation as consistency-based semi-supervised learning. Our key contributions are the simplicity and effectiveness of our method for training a single model to produce high quality depth estimates in the unlabelled target domain, based on the consistency of the predictions under different input augmentations. The proposed joint optimisation of the source and target domains with the proposed perturbation consistency loss and the pairwise source loss functions simplifies the training process compared to previous work that relies on complex training protocols and uses more than a single model. In our experiments, we showed promising results on the KITTI and NYUv2 datasets, which are considered standard for the domain adaptation task in monocular depth estimation.

## 6 ACKNOWLEDGEMENTS

Part of the research leading to these results is funded by the German Research Foundation (DFG) within the project 458972748. The authors would like to thank the foundation for the successful cooperation.

Additionally the authors gratefully acknowledge the scientific support and HPC resources provided by the Erlangen National High Performance Computing Center (NHR@FAU) of the Friedrich-Alexander-Universität Erlangen-Nürnberg (FAU). The hardware is funded by the German Research Foundation (DFG).

## REFERENCES

Ashutosh Agarwal and Chetan Arora. Attention attention everywhere: Monocular depth prediction with skip attention. In *Proceedings of the IEEE/CVF Winter Conference on Applications of Computer Vision*, pp. 5861–5870, 2023.

- Hiroyasu Akada, Shariq Farooq Bhat, Ibraheem Alhashim, and Peter Wonka. Self-supervised learning of domain invariant features for depth estimation. In *Proceedings of the IEEE/CVF Winter Conference on Applications of Computer Vision*, pp. 3377–3387, 2022.
- Ali Jahani Amiri, Shing Yan Loo, and Hong Zhang. Semi-supervised monocular depth estimation with left-right consistency using deep neural network. In *2019 IEEE International Conference on Robotics and Biomimetics (ROBIO)*, pp. 602–607, 2019. doi: 10.1109/ROBIO49542.2019.8961504.
- Amir Atapour Abarghouei and Toby Breckon. Real-time monocular depth estimation using synthetic data with domain adaptation via image style transfer. pp. 2800–2810, 06 2018. doi: 10.1109/CVPR.2018.00296.
- David Berthelot, Nicholas Carlini, Ekin D Cubuk, Alex Kurakin, Kihyuk Sohn, Han Zhang, and Colin Raffel. Remix-match: Semi-supervised learning with distribution matching and augmentation anchoring. In *International Conference on Learning Representations*, 2019.
- Shariq Farooq Bhat, Ibraheem Alhashim, and Peter Wonka. Adabins: Depth estimation using adaptive bins. In *Proceedings of the IEEE/CVF Conference on Computer Vision and Pattern Recognition*, pp. 4009–4018, 2021.
- Yuanzhouhan Cao, Zifeng Wu, and Chunhua Shen. Estimating Depth from Monocular Images as Classification Using Deep Fully Convolutional Residual Networks, May 2016. URL <https://arxiv.org/abs/1605.02305v3>.
- Mathilde Caron, Ishan Misra, Julien Mairal, Priya Goyal, Piotr Bojanowski, and Armand Joulin. Unsupervised learning of visual features by contrasting cluster assignments. *Advances in neural information processing systems*, 33: 9912–9924, 2020.
- Xiaotian Chen, Yuwang Wang, Xuejin Chen, and Wenjun Zeng. S2r-depthnet: Learning a generalizable depth-specific structural representation. In *Proceedings of the IEEE/CVF conference on computer vision and pattern recognition*, pp. 3034–3043, 2021.
- Yun-Chun Chen, Yen-Yu Lin, Ming-Hsuan Yang, and Jia-Bin Huang. Crdoco: Pixel-level domain transfer with cross-domain consistency. In *Proceedings of the IEEE/CVF conference on computer vision and pattern recognition*, pp. 1791–1800, 2019.
- Ekin D. Cubuk, Barret Zoph, Jonathon Shlens, and Quoc V. Le. RandAugment: Practical automated data augmentation with a reduced search space, November 2019. URL <http://arxiv.org/abs/1909.13719>. arXiv:1909.13719 [cs].
- David Eigen, Christian Puhrsch, and Rob Fergus. Depth Map Prediction from a Single Image using a Multi-Scale Deep Network, June 2014. URL <http://arxiv.org/abs/1406.2283>. arXiv:1406.2283 [cs].
- Huan Fu, Mingming Gong, Chaohui Wang, Kayhan Batmanghelich, and Dacheng Tao. Deep Ordinal Regression Network for Monocular Depth Estimation, June 2018. URL <https://arxiv.org/abs/1806.02446v1>.
- Adrien Gaidon, Qiao Wang, Yohann Cabon, and Eleonora Vig. Virtual Worlds as Proxy for Multi-Object Tracking Analysis, May 2016. URL <http://arxiv.org/abs/1605.06457>. arXiv:1605.06457 [cs, stat].
- Ravi Garg, Vijay Kumar Bg, Gustavo Carneiro, and Ian Reid. Unsupervised cnn for single view depth estimation: Geometry to the rescue. In *Computer Vision—ECCV 2016: 14th European Conference, Amsterdam, The Netherlands, October 11–14, 2016, Proceedings, Part VIII 14*, pp. 740–756. Springer, 2016.
- Andreas Geiger, P Lenz, Christoph Stiller, and Raquel Urtasun. Vision meets robotics: the KITTI dataset. *The International Journal of Robotics Research*, 32:1231–1237, September 2013. doi: 10.1177/0278364913491297.
- Clément Godard, Oisín Mac Aodha, and Gabriel J Brostow. Unsupervised monocular depth estimation with left-right consistency. In *Proceedings of the IEEE conference on computer vision and pattern recognition*, pp. 270–279, 2017.
- Ankur Handa, Viorica Patraucean, Vijay Badrinarayanan, Simon Stent, and Roberto Cipolla. SceneNet: Understanding Real World Indoor Scenes With Synthetic Data, November 2015. URL <http://arxiv.org/abs/1511.07041>. arXiv:1511.07041 [cs].
- Julia Hornauer and Vasileios Belagiannis. Gradient-based Uncertainty for Monocular Depth Estimation, August 2022. URL <http://arxiv.org/abs/2208.02005>. arXiv:2208.02005 [cs].

- Julia Hornauer, Lazaros Nalpantidis, and Vasileios Belagiannis. Visual domain adaptation for monocular depth estimation on resource-constrained hardware. *CoRR*, abs/2108.02671, 2021. URL <https://arxiv.org/abs/2108.02671>.
- Diederik P. Kingma and Jimmy Ba. Adam: A method for stochastic optimization. *CoRR*, abs/1412.6980, 2014. URL <https://api.semanticscholar.org/CorpusID:6628106>.
- Jogendra Kundu, Phani Krishna Uppala, Anuj Pahuja, and R. Babu. Adadepth: Unsupervised content congruent adaptation for depth estimation. 03 2018.
- Yevhen Kuznetsov, Jorg Stuckler, and Bastian Leibe. Semi-supervised deep learning for monocular depth map prediction. In *Proceedings of the IEEE conference on computer vision and pattern recognition*, pp. 6647–6655, 2017.
- Iro Laina, Christian Rupprecht, Vasileios Belagiannis, Federico Tombari, and Nassir Navab. Deeper depth prediction with fully convolutional residual networks. In *2016 Fourth international conference on 3D vision (3DV)*, pp. 239–248. IEEE, 2016.
- Zhixuan Lin, Yi-Fu Wu, Skand Vishwanath Peri, Weihao Sun, Gautam Singh, Fei Deng, Jindong Jiang, and Sungjin Ahn. Space: Unsupervised object-oriented scene representation via spatial attention and decomposition. *arXiv preprint arXiv:2001.02407*, 2020.
- Ce Liu, Suryansh Kumar, Shuhang Gu, Radu Timofte, and Luc Van Gool. Va-depthnet: A variational approach to single image depth prediction, 2023.
- Fayao Liu, Chunhua Shen, Guosheng Lin, and Ian Reid. Learning Depth from Single Monocular Images Using Deep Convolutional Neural Fields. *IEEE Transactions on Pattern Analysis and Machine Intelligence*, 38(10): 2024–2039, October 2016. ISSN 0162-8828, 2160-9292. doi: 10.1109/TPAMI.2015.2505283. URL <http://arxiv.org/abs/1502.07411>. arXiv:1502.07411 [cs].
- Adrian Lopez-Rodriguez and Krystian Mikolajczyk. DESC: Domain Adaptation for Depth Estimation via Semantic Consistency, September 2020. URL <http://arxiv.org/abs/2009.01579>. arXiv:2009.01579 [cs].
- Reza Mahjourian, Martin Wicke, and Anelia Angelova. Unsupervised learning of depth and ego-motion from monocular video using 3d geometric constraints. In *Proceedings of the IEEE conference on computer vision and pattern recognition*, pp. 5667–5675, 2018.
- Pushmeet Kohli Nathan Silberman, Derek Hoiem and Rob Fergus. Indoor segmentation and support inference from rgb-d images. In *ECCV*, 2012.
- Hyeseung Park and Seungchul Park. An unsupervised depth-estimation model for monocular images based on perceptual image error assessment. *Applied Sciences*, 12(17), 2022. ISSN 2076-3417. doi: 10.3390/app12178829. URL <https://www.mdpi.com/2076-3417/12/17/8829>.
- Peng Wang, Xiaohui Shen, Zhe Lin, Scott Cohen, Brian Price, and Alan Yuille. Towards unified depth and semantic prediction from a single image. In *2015 IEEE Conference on Computer Vision and Pattern Recognition (CVPR)*, pp. 2800–2809, Boston, MA, USA, June 2015. IEEE. ISBN 978-1-4673-6964-0. doi: 10.1109/CVPR.2015.7298897. URL <http://ieeexplore.ieee.org/document/7298897/>.
- Koutilya PNVR, Hao Zhou, and David Jacobs. SharinGAN: Combining Synthetic and Real Data for Unsupervised Geometry Estimation, June 2020. URL <http://arxiv.org/abs/2006.04026>. arXiv:2006.04026 [cs].
- Weichao Qiu and Alan Yuille. Unrealcv: Connecting computer vision to unreal engine. In *Computer Vision—ECCV 2016 Workshops: Amsterdam, The Netherlands, October 8–10 and 15–16, 2016, Proceedings, Part III 14*, pp. 909–916. Springer, 2016.
- René Ranftl, Alexey Bochkovskiy, and Vladlen Koltun. Vision transformers for dense prediction. In *Proceedings of the IEEE/CVF international conference on computer vision*, pp. 12179–12188, 2021.
- Olaf Ronneberger, Philipp Fischer, and Thomas Brox. U-Net: Convolutional Networks for Biomedical Image Segmentation. *Lecture Notes in Computer Science*, pp. 234–241, Cham, 2015. Springer International Publishing. ISBN 978-3-319-24574-4. doi: 10.1007/978-3-319-24574-4\_28.
- Michael Rudolph, Youssef Dawoud, Ronja G ldenring, Lazaros Nalpantidis, and Vasileios Belagiannis. Lightweight monocular depth estimation through guided decoding, 2022.



- Ashutosh Saxena, Min Sun, and Andrew Ng. Make3d: Learning 3d scene structure from a single still image. *IEEE transactions on pattern analysis and machine intelligence*, 31:824–40, 06 2009. doi: 10.1109/TPAMI.2008.132.
- Ashish Shrivastava, Tomas Pfister, Oncel Tuzel, Joshua Susskind, Wenda Wang, and Russell Webb. Learning from simulated and unsupervised images through adversarial training. In *Proceedings of the IEEE conference on computer vision and pattern recognition*, pp. 2107–2116, 2017.
- Kihyuk Sohn, David Berthelot, Nicholas Carlini, Zizhao Zhang, Han Zhang, Colin A Raffel, Ekin Dogus Cubuk, Alexey Kurakin, and Chun-Liang Li. Fixmatch: Simplifying semi-supervised learning with consistency and confidence. *Advances in neural information processing systems*, 33:596–608, 2020.
- Zitang Sun, Shin’ya Nishida, and Zhengbo Luo. Unsupervised learning optical flow in multi-frame dynamic environment using temporal dynamic modeling. *arXiv preprint arXiv:2304.07159*, 2023.
- Yang Wang, Yi Yang, Zhenheng Yang, Liang Zhao, Peng Wang, and Wei Xu. Occlusion aware unsupervised learning of optical flow. In *Proceedings of the IEEE conference on computer vision and pattern recognition*, pp. 4884–4893, 2018.
- Yidong Wang, Hao Chen, Qiang Heng, Wenxin Hou, Yue Fan, Zhen Wu, Jindong Wang, Marios Savvides, Takahiro Shinozaki, Bhiksha Raj, et al. Freematch: Self-adaptive thresholding for semi-supervised learning. *arXiv preprint arXiv:2205.07246*, 2022.
- Junyan Xie, Linli Xu, and Enhong Chen. Deep3d: Fully automatic 2d-to-3d video conversion with deep convolutional neural networks. In *AAAI*, pp. 542–548, 2016.
- Lihe Yang, Lei Qi, Litong Feng, Wayne Zhang, and Yinghuan Shi. Revisiting weak-to-strong consistency in semi-supervised semantic segmentation. In *Proceedings of the IEEE/CVF Conference on Computer Vision and Pattern Recognition*, pp. 7236–7246, 2023.
- Yu-Ting Yen, Chia-Ni Lu, Wei-Chen Chiu, and Yi-Hsuan Tsai. 3D-PL: Domain Adaptive Depth Estimation with 3D-aware Pseudo-Labeling, September 2022. URL <http://arxiv.org/abs/2209.09231>. arXiv:2209.09231 [cs].
- Wei Yin, Yifan Liu, Chunhua Shen, and Youliang Yan. Enforcing geometric constraints of virtual normal for depth prediction, July 2019. URL <https://arxiv.org/abs/1907.12209v2>.
- Zhichao Yin, Jianping Shi, Hui Li, Xiaogang Dai, and Xinchao Lin. Geonet: Unsupervised learning of dense depth, optical flow and camera pose. In *Proceedings of the IEEE Conference on Computer Vision and Pattern Recognition*, pp. 1983–1992, 2018.
- Weihaio Yuan, Xiaodong Gu, Zuozhuo Dai, Siyu Zhu, and Ping Tan. New crfs: Neural window fully-connected crfs for monocular depth estimation. *arXiv preprint arXiv:2203.01502*, 2022.
- Sangdoo Yun, Dongyoon Han, Seong Joon Oh, Sanghyuk Chun, Junsuk Choe, and Youngjoon Yoo. CutMix: Regularization Strategy to Train Strong Classifiers with Localizable Features, August 2019. URL <http://arxiv.org/abs/1905.04899>. arXiv:1905.04899 [cs].
- Bowen Zhang, Yidong Wang, Wenxin Hou, Hao Wu, Jindong Wang, Manabu Okumura, and Takahiro Shinozaki. Flexmatch: Boosting semi-supervised learning with curriculum pseudo labeling. *Advances in Neural Information Processing Systems*, 34:18408–18419, 2021.
- Shanshan Zhao, Huan Fu, Mingming Gong, and Dacheng Tao. Geometry-Aware Symmetric Domain Adaptation for Monocular Depth Estimation, April 2019. URL <http://arxiv.org/abs/1904.01870>. arXiv:1904.01870 [cs].
- Chuanxia Zheng, Tat-Jen Cham, and Jianfei Cai. T2Net: Synthetic-to-Realistic Translation for Solving Single-Image Depth Estimation Tasks, August 2018. URL <http://arxiv.org/abs/1808.01454>. arXiv:1808.01454 [cs].
- Tinghui Zhou, Matthew Brown, Noah Snavely, and David G Lowe. Unsupervised learning of depth and ego-motion from video. In *Proceedings of the IEEE Conference on Computer Vision and Pattern Recognition*, pp. 6619–6627, 2017.
- Yuliang Zou, Zelun Luo, and Jia-Bin Huang. Df-net: Unsupervised joint learning of depth and flow using cross-task consistency. In *Proceedings of the European conference on computer vision (ECCV)*, pp. 36–53, 2018.

## A APPENDIX

### A.1 METRICS

We use the common evaluation metrics used for several depth estimation benchmarks and established by [Eigen et al. \(2014\)](#). These include:

- Root Mean Squared Error (RMSE):

$$RMSE = \sqrt{\frac{1}{N} \sum_{i=1}^N \|d_i - \hat{d}_i\|^2} \quad (10)$$

- RMSE log:

$$RMSE_{log} = \sqrt{\frac{1}{N} \sum_{i=1}^N \|\log d_i - \log \hat{d}_i\|^2} \quad (11)$$

- Squared Relative Error (Sq Rel):

$$SqRel = \frac{1}{N} \sum_{i=1}^N \frac{\|d_i - \hat{d}_i\|^2}{d_i^2} \quad (12)$$

- Absolute Relative Error (Abs Rel):

$$AbsRel = \frac{1}{N} \sum_{i=1}^N \frac{|d_i - \hat{d}_i|}{d_i} \quad (13)$$

- Accuracy under threshold  $\delta$ :

$$Accuracy_{\delta} = \frac{1}{N} \sum_{i=1}^N I(|\hat{d}_i - d_i| < (d_i * \delta)) \quad (14)$$

Where  $d_i$  is the ground truth depth,  $\hat{d}_i$  is the estimated depth,  $N$  is the total number of samples, and  $I(\cdot)$  is an indicator function that returns 1 if the condition holds, 0 otherwise. In the experimental results A1 refers to  $\delta < 1.25$ , A2 to  $\delta < 1.25^2$  and A3 to  $\delta < 1.25^3$ .

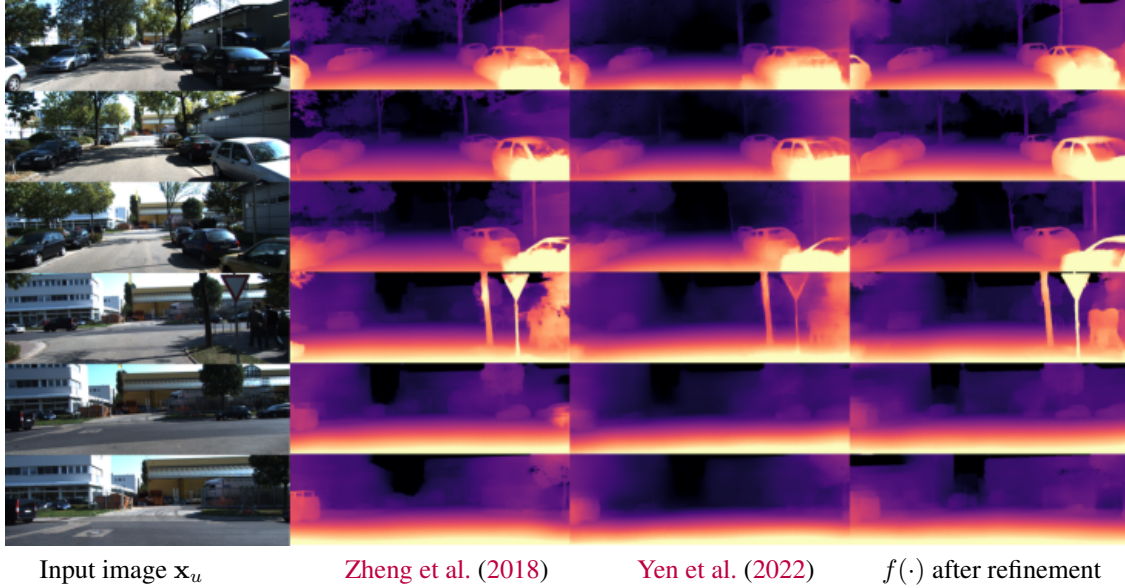
### A.2 PRETRAINING

During pretraining, we solely use source domain data  $D_S$  to train the depth estimation model  $f(\cdot)$ . The following sections explain hyperparameter adjustment for the proposed pretraining approach and provide more information on the used augmentations during pretraining.

**CutMix Hyperparameter  $\alpha$**  We use a hyperparameter of  $\alpha = 0.5$  to balance the information between the original and augmented images during CutMix ([Yun et al., 2019](#)). This ratio was chosen so that the model would not be overwhelmed by drastic augmentations, as monocular depth estimation requires an understanding of the surrounding scene context. With  $\alpha = 0.5$ , patches from the two input images are mixed approximately equally, providing additional cues about depth relationships while still retaining most of the original scene structure.

**Other augmentations** In addition to CutMix augmentations during the pre-training, we also employ standard color and geometric data augmentation techniques. Color augmentations, including random jitter, are applied to expose the model to variations in colorspace. Furthermore, geometric transformations such as random rotations are utilised. This can be seen in Fig. 5.

**Quantitative results** Our findings demonstrate that models pre-trained using the augmentation pipeline incorporating CutMix, randomised colorspace jittering, and geometric rotations produce improved depth predictions compared to networks exclusively optimised on the labeled vKITTI source data without augmentations (see Tab. 7). However, quantitative evaluation reveals the proposed approach does not achieve a performance similar to state-of-the-art methods for monocular depth estimation in unsupervised domain adaptation.

Figure 5: CutMix augmented images with random jitter and rotation augmentations in  $D_S$  for images in vKITTI.Figure 6: Additional qualitative results on KITTI eigen test samples  $x_u$  between other state-of-the-art models.

**Qualitative results** Further qualitative results in the pretraining stage, where the model  $f(\cdot)$  is only trained on heavily augmented source data in  $D_S$ , can be seen in Fig. 7. A comparison between the pretrained  $f(\cdot)$  and  $f(\cdot)$  after the proposed approach shows a clear smoothing effect of our approach. Sharp discontinuities present in the boundary regions of the pretrained  $f(\cdot)$  maps are noticeably attenuated after refinement. This indicates the model  $f(\cdot)$  learns to produce depth outputs that align more smoothly across pixel neighbours after leveraging both labelled source data and unlabelled target images during refinement.

Table 7: Depth estimation performance of our model  $f(\cdot)$  after the pretraining in  $D_S$ .  $f(\cdot)$  is trained on vKITTI only and tested on KITTI (50m cap). Different augmentation pipelines are compared.

Augmentations	AbsRel↓	SqRel↓	RMSE↓	RMSE log↓	A1↑	A2↑	A3↑
None	0.244	1.771	5.354	0.313	0.647	0.866	0.943
CutMix, rotations, jitter	0.173	1.413	5.062	0.264	0.767	0.906	0.957
Rotations, jitter	0.187	1.538	5.104	0.266	0.756	0.901	0.958

**Training process** During refinement, both the source ( $D_S$ ) and target ( $D_T$ ) datasets are jointly used to update the monocular depth estimation model  $f(\cdot)$ . To augment the training data, we apply a combination of various techniques, which will be discussed in the following section. Subsequently, we provide more qualitative results. Finally, we present details on the computational resources required for the refinement process.

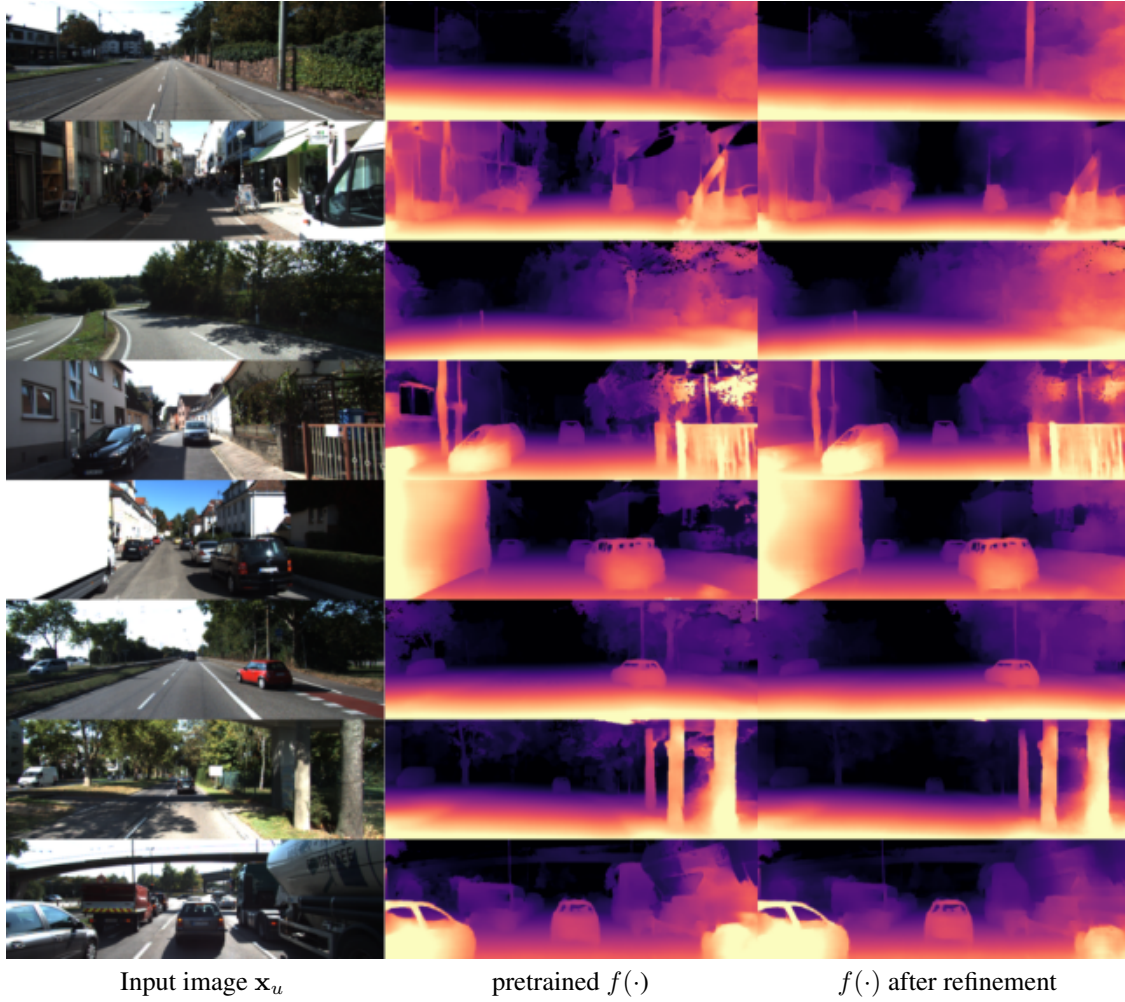


Figure 7: Comparison of depth predictions on KITTI eigen test samples  $x_u$ , after pretraining (middle column) and after refinement (right column).



### A.3 FURTHER ABLATION STUDIES

**Number of perturbations in  $\mathcal{L}_{cons}^t$**  To explore the effect of increasing target domain perturbations, we conduct an experiment varying the number of augmentation streams applied to target samples (see Tab. 8). Specifically, we evaluate model performance when employing two, three and four independent RandAugment (Cubuk et al., 2019) augmentations of target samples simultaneously as multi-stream perturbations during training, in addition to the pairwise supervised source loss  $\mathcal{L}_{\Sigma}^s$ .

Table 8: Comparison of required GPU memory and performance metrics for two, three and four perturbations of target images for the target loss  $\mathcal{L}_{cons}^t$ .

# of perturbations	required GPU memory	Abs Rel↓	A1↑
2	30GB	0.165	0.779
3	35GB	<b>0.161</b>	0.785
4	40GB	<b>0.161</b>	<b>0.786</b>

It should be noted that we calculate the number of perturbations by counting each augmented sample alongside its corresponding original, non-augmented counterpart. For example, to obtain a total of three perturbations, we employ one baseline image paired with two transformed views. Our experiments revealed that the quantity of perturbations applied to target domain data has a substantial impact on the efficacy of the proposed approach. While gains were observed for all perturbation counts investigated, performance improvements became more pronounced with more than two augmented samples. Peak results were attained with three perturbations, as evidenced by our key evaluation metrics. As incorporating additional perturbations linearly increases computational overhead and memory requirements, we opted to use the three-perturbation setting due to its trade-off between achieved accuracy and demanded resources.

**Training time in comparison to other approaches** To facilitate quantitative comparison of computational requirements, we conducted an ablation analysis reporting training time and number of models for our method and relevant baselines. Since training duration scales with the number of models optimized as well as their architectures, we record both the total time spent training and the additional models employed beyond our approach. Across all experiments, we log two performance metrics (see Tab. 9).

Table 9: Comparison of the proposed approach with other methods in terms of the total training time, the number of additionally trained models and two performance metrics.

Method	Total training time	# of trainable models	Abs Rel↓	A2↑
Ours	≈6h	1	0.161	0.918
Zheng et al. (2018)	≈8h	3	0.168	0.912
Yen et al. (2022)	-	2	0.162	0.916
Lopez-Rodriguez & Mikolajczyk (2020)	≈18h	3	0.161	0.915

Due to the unavailability of training code from 3D-PL (Yen et al., 2022), we could not directly replicate their model optimization procedure and thus cannot report their total training time. While DESC (Lopez-Rodriguez & Mikolajczyk, 2020) attains markedly better results than other referenced techniques, it employs a multi-stage pipeline incorporating additional models for object detection, sim-to-real translation, and depth estimation. Remarkably, our proposed method outperforms all prior work across standard evaluation metrics for this task while retaining a highly efficient single-model formulation.

**Significance of  $\mathcal{L}_{\Sigma}^s$**  We conduct additional ablation experiments to further evaluate the impact of our proposed pairwise source loss  $\mathcal{L}_{\Sigma}^s$  (see Tab. 10). First, we compare the standard per-sample  $\mathcal{L}_1$  loss ( $\mathcal{L}_1^s(\hat{y}_{s,1}, y_{s,1})$ ) against our pairwise formulation. Secondly, we independently apply the pairwise loss ( $\mathcal{L}_{\Sigma,sep}^s = \mathcal{L}_1(\hat{y}_{s,1}, y_{s,1}) + \mathcal{L}_1(\hat{y}_{s,2}, y_{s,2})$ ) without jointly optimising the samples.

All experiments utilise three target domain perturbations for consistency regularisation, to isolate the effects of varying only the source supervision approach.

Across all experiments utilising the source loss  $\mathcal{L}^s$ , we observed a regularising effect relative to omitting source supervision entirely. However, upon closer inspection, the Abs Rel and Sq Rel error metrics revealed a notable performance gap. Specifically, the pairwise loss  $\mathcal{L}_{\Sigma}^s$  substantially outperformed the standard per-sample  $\mathcal{L}_1^s$  and independently applied pairwise  $\mathcal{L}_{\Sigma,sep}^s$  variants.

Table 10: Comparison of different implementations for the source loss.

source loss	AbsRel↓	SqRel↓	RMSE↓	RMSE log↓	A1↑	A2↑	A3↑
no source loss	0.171	1.178	4.544	0.248	0.781	0.912	0.965
$\mathcal{L}_{\sum}^s$	0.161	1.028	4.449	0.237	0.785	0.918	0.968
$\mathcal{L}_1^s$	0.167	1.143	4.468	0.241	0.783	0.913	0.965
$\mathcal{L}_{\sum,sep}^s$	0.164	1.109	4.491	0.241	0.781	0.912	0.966

**Hyperparameter selection** Given the lack of depth annotations in the target domain, we required an unsupervised method to assess prediction performance without ground truth labels. Gradient-based uncertainty estimation (Hornauer & Belagiannis, 2022) allows for such an evaluation under this unlabelled setting.

By approximating a model’s uncertainty through perturbations and gradients, this technique enables quantification of a prediction’s ambiguity even without a labelled target. As our goal was to validate the quality and reliability of our estimated depth maps for the unlabelled target domain, we opted to apply this approach.

The hyperparameters ( $r$ , learning rate, number of epochs) were optimised via predictive uncertainty estimation of the trained models. Models trained with various hyperparameter values were evaluated, model selection was then based on minimizing average estimated uncertainty.

Specifically, we generated reference depth predictions by augmenting inputs through horizontal flipping (Hornauer & Belagiannis, 2022). To approximate uncertainty, gradients of the convolutional blocks within the UNet-based depth estimation network, particularly in the expansion phase, were extracted.

We performed gradient-based uncertainty analysis on the KITTI Eigen validation split comprising 888 to evaluate outdoor performance. For indoors, we applied the uncertainty estimation to a held-out 1000 image NYUv2 subset, both unseen during training.

#### A.4 TRAINING PROCESS IN $D_T$

To gain deeper insights, ablation experiments are also conducted investigating the impact of perturbations applied via RandAugment (Cubuk et al., 2019) multi-stream consistency regularisation. RandAugment utilises randomly composed augmentations parameterised by the augmentation set  $S$ , depth  $n$  and severity  $m$ . Specifically, we analyse variations in these hyperparameters which control the RandAugment transformations enforcing predictive consistency between augmented unlabelled target samples. The parameters studied include the augmentation set  $S$  from which augmentations are selected, as well as the ranges  $n$  and  $m$  defining the permissible number and strength of augmentations in a random augmentation chain. Our default augmentation set is similar to the configuration presented in the FixMatch (Sohn et al., 2020) literature, though we additionally evaluate removing geometric transforms to analyse their contribution. The official augmentation set  $s_{fm}$  used in FixMatch are:

```
s_fm = [AutoContrast(),
        Brightness(),
        Color(),
        Contrast(),
        Equalize(),
        Identity(),
        Posterize(),
        Rotate(),
        Sharpness(),
        ShearX(),
        ShearY(),
        Solarize(),
        TranslateX(),
        TranslateY()]
```

In our ablation studies we removed all geometric augmentation, such that  $s_{geo}$ :

```
s_geo = [AutoContrast(),
        Brightness(),
        Color(),
        Contrast(),
        Equalize(),
        Identity(),
```

Table 11: Comparison of the refinement process trained on vKITTI-KITTI and tested on the KITTI eigen split (capped to 50m), depending on the augmentation set  $s$ , depth  $n$  and severity  $m$  of the augmentation in  $D_T$ .

$s$	$n$	$m$	AbsRel↓	SqRel↓	RMSE↓	RMSE log↓	A1↑	A2↑	A3↑
$s_{geo}$	1	5	0.172	1.164	4.490	0.244	0.781	0.916	0.966
$s_{fm}$	1	5	0.169	1.087	<b>4.428</b>	0.239	0.783	0.917	0.967
$s_{fm}$	5	7	0.173	1.123	4.41	0.242	0.781	0.916	0.966
$s_{fm}$	1	7	<b>0.161</b>	<b>1.028</b>	4.449	<b>0.237</b>	<b>0.785</b>	<b>0.918</b>	<b>0.968</b>

```

Posterize(),
Sharpness(),
Solarize()]

```

In Tab. 11 the performance of the depth estimation model  $f(\cdot)$  is compared in multiple variations of the hyperparameters  $s, n$  and  $m$ . The results indicate that the augmentation set  $s_{geo}$  is outperformed by  $s_{fm}$ . The best performance is given for the parameter combination  $s = s_{fm}, n = 1$  and  $m = 7$  although performance gaps in general are minor for parameters within  $s_{fm}$ . During our analysis of the augmented data, we observed that for the parameter setting of the depth parameter  $n = 1$ , the transformations sometimes did not perturb the input at all, limiting their regularisation effect. To address this, we introduce a static CutOut augmentation applied to the input images prior to the other transformations.

**Qualitative results** To further evaluate our approach on more complex KITTI scenes, Fig. 6 compares our refined model  $f(\cdot)$  to other state-of-the-art methods using denser samples from the KITTI eigen test split. Qualitatively, our method produces depth maps that better preserve fine structural details throughout the scenes.

Prior work tends to oversmooth object boundaries and thin structures such as street signs. In contrast,  $f(\cdot)$  trained with our domain adaptation framework more sharply smoothes objects at boundaries while still maintaining consistent predictions. This indicates its capability to balance high-frequency content with regularizing across image domains  $D_S$  and  $D_T$ .

To further demonstrate the effectiveness of our approach in indoor scenes, we present qualitative evaluations on the NYUv2 (Nathan Silberman & Fergus, 2012) eigen test set (Eigen et al., 2014) in Fig. 8. Similar to the outdoor KITTI results, our method preserves fine-scale structural details that prior methods often overlook.

For example, as shown in the first row of Fig. 8, our predicted depth maps are able to sharply identify objects like toilet seats with thin structures. Additionally, Fig. 8 shows that our approach accurately infers the scene layout while also capturing small objects such as a desk lamp against complex indoor backgrounds.

**Hardware requirements** Empirically, we found a ratio parameter  $r = 2$  performed best across indoor and outdoor scenes. With a batch size  $N$  of 12, the concatenated inputs contain  $N_{concat} = 42$  images as:

$$N_{concat} = \underbrace{3 \times N \times \frac{1}{r}}_{[x_u, \tilde{x}_{u,1}, \tilde{x}_{u,2}] \in D_T} + \underbrace{2 \times N \times r}_{[x_{s,1}, x_{s,2}] \in D_S} \Big|_{r=2, b=12} \quad (15)$$

For KITTI resized to 640x192, this requires 35GB of GPU memory. With NYUv2 at 256x192, memory usage is 20GB.

Higher resolutions increase memory cost due to redundant feature representations. We also tested varying  $N$ , but larger batches exceed GPU limits whereas smaller  $N$  weakened the overall regularisation effect. Given hardware constraints, the above configuration provides the optimal trade-off between batch size, memory requirements, and regularisation effect during our refinement approach.



Figure 8: Qualitative results on NYUv2 eigen test samples  $x_u$  to another state-of-the-art model. Both models were trained in the indoor domain adaptation setting (SceneNet-NYUv2) and are evaluated on NYUv2 eigen test samples.